

## OPTICS

## Solid state–like high harmonic generation from cluster molecules with rotational periodicities

Yigeng Peng<sup>1</sup>, Tong Wu<sup>1</sup>, Guanglu Yuan<sup>1</sup>, Lihan Chi<sup>1</sup>, Shicheng Jiang<sup>1,2</sup>, Konstantin Dorfman<sup>2,3,4,5\*</sup>, Chao Yu<sup>1\*</sup>, Ruifeng Lu<sup>1,6\*</sup>

High harmonic generation (HHG) from solid-state crystals in strong laser fields has been understood by the band structure of the solids, which is based on the periodic boundary condition (PBC) due to translational invariance. For the systems with PBC due to rotational invariance, an analogous Bloch theorem can be applied. Considering a ring-type cluster of cyclo[18]carbon as an example, we develop a quasi-band model and predict the solid state–like HHG in this system. Under the irradiation of linearly polarized laser field, cyclo[18]carbon exhibits solid state–like HHG originated from intraband oscillations and interband transitions, which, in turn, is promising to optically detect the symmetry and geometry of molecular or material structures. Our results based on the Liouville–von Neumann equations are well reproduced by the time-dependent density functional theory calculations and are foundational in providing a connection linking the HHG physics of gases and solids.

## INTRODUCTION

In the past decades, the high harmonic generation (HHG) of gaseous media with the interaction of a driving strong laser has been extensively studied for its potential applications in optical technology, such as attosecond pulse generation and spectral characterization of structural or electronic dynamics (1). In the meantime, the “ionization-acceleration-recombination” three-step model (2) has been widely recognized. Limited by the density of gaseous targets, the harmonic conversion efficiency is dissatisfactory for widespread usage. Because of the high density of atoms in solids, efficient high harmonics from crystalline bulk and two-dimensional materials have been observed in recent years (3, 4). In this emerging field, many interesting phenomena have been reported, including intraband Bloch oscillation (3), interband interference (5), atomic-like HHG (6, 7), and even-order harmonics due to symmetry breaking of crystal structure (8, 9). On the other hand, the cutoff energy of solid-state HHG is limited by materials’ damage thresholds under the irradiation of a strong laser beam. A molecular cluster that is normally composed of several (up to tens of thousands) atoms could be regarded as the intermediate system between the atom and the solid material that has both atomic and solid-state characteristics. The HHG properties of noble gas clusters are found to be special, e.g., the higher cutoff energy and the lower decay rate when the cluster size gets larger (10) and the nonquadratic law of HHG yield in terms of the atomic density (11). However, all previous HHG studies in molecular clusters are based on the three-step model, which are similar to atomic

systems: An electron is first ionized and accelerated by the laser field, then returns and recombines with the mother cation when the electric field changes sign, and finally emits high-energy photons. In comparison with atoms, the enhancement of HHG from clusters is due to the fact that the delocalized electronic wave function leads to larger polarizability and higher recollision probability.

Here, we use the symmetric properties of the molecular crystals to define periodic boundary conditions (PBCs) that make the cluster description similar to that of a solid-state crystal. By considering the physical analogy between crystals with translational PBC and ring-type systems with rotational PBC, in this work, we propose a solid state–like HHG mechanism of ring-type cluster cyclo[18]-carbon in the framework of a generalized Bloch theorem with rotational PBC.

For solid crystals, electron delocalization in lattice structure can be described by the PBC due to the translational invariance. As shown in Fig. 1, another kind of PBC can be obtained from the rotational invariance. For ring-type systems of  $N$ -fold rotational symmetry, similar to the translational invariance in ordered solids, their eigenfunctions satisfy a generalized Bloch theorem (12–14), which is suggested as

$$\psi_J(\theta + \theta_0) = \psi_J(\theta) \cdot e^{ij\theta_0} \quad (1)$$

where  $\theta_0 = 2\pi/N$  represents the rotation angle that makes the system rotational invariant.  $J$  should be an integer according to the boundary condition:  $\psi_J(\theta + 2\pi) = \psi_J(\theta)$  and  $\psi_J = \psi_{J+N}$ , which means that only  $N$  independent values of  $J$  are available. Equation 1 enables the electron delocalization in ring-type systems. Analogous to crystalline solids, the physical quantity  $J$  here can be regarded as some kind of angular momentum because of the rotational invariability by certain angles, which is similar to the crystal momentum of solids due to the translational invariability by certain vectors. Meanwhile,  $N$  can be regarded as a reciprocal lattice vector, and the region of  $J$  values comprises the effective Brillouin zone (quasi-reciprocal space). Then, a quasi–energy band structure can be obtained by combining the eigen-energies of all  $J$ , as shown in Fig. 2A.

<sup>1</sup>Institute of Ultrafast Optical Physics, Department of Applied Physics, and MIIT Key Laboratory of Semiconductor Microstructure and Quantum Sensing, Nanjing University of Science and Technology, Nanjing 210094, China. <sup>2</sup>State Key Laboratory of Precision Spectroscopy, East China Normal University, Shanghai 200062, China. <sup>3</sup>Center for Theoretical Physics and School of Sciences, Hainan University, Haikou 570228, China. <sup>4</sup>Collaborative Innovation Center of Extreme Optics, Shanxi University, Taiyuan, Shanxi 030006, China. <sup>5</sup>Himalayan Institute for Advanced Study, Unit of Gopinath Seva Foundation, MIG 38, Avas Vikas, Rishikesh, Uttarakhand 249201, India. <sup>6</sup>State Key Laboratory of Molecular Reaction Dynamics, Dalian Institute of Chemical Physics, Chinese Academy of Sciences, Dalian 116023, China.

\*Corresponding author. Email: dorfman@lps.ecnu.edu.cn (K.D.); chaoyu@njust.edu.cn (C.Y.); rflu@njust.edu.cn (R.L.)

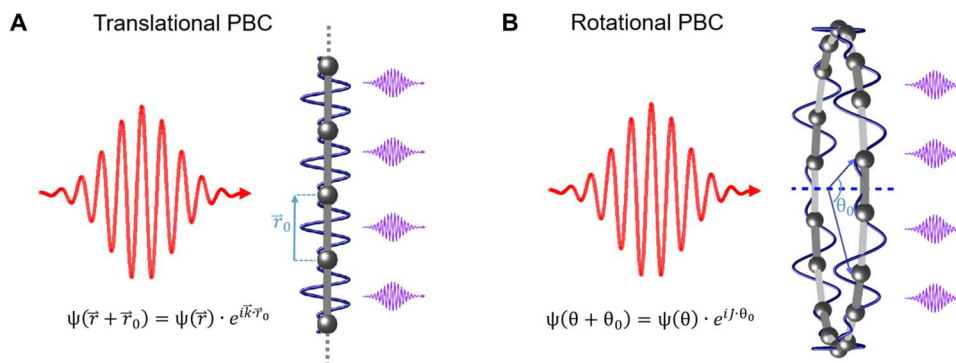


**Fig. 1. Schematic of the generalized Bloch theorem for the systems.** (A) For the systems with translational PBC, the eigenfunctions obey the Bloch theorem with the translational invariance, and a highly nonlinear optical effect such as HHG (in purple) could be induced under the irradiation of an intense laser (in red), which can be simulated by solving semiconductor Bloch equations based on the band theory of solid. (B) For the systems with rotational PBC, the eigenfunctions follow a similar Bloch theorem with the rotational invariance, and high-order harmonics (in purple) could be emitted with interaction of an intense laser (in red), which can be studied by a quasi-band model proposed in this work.

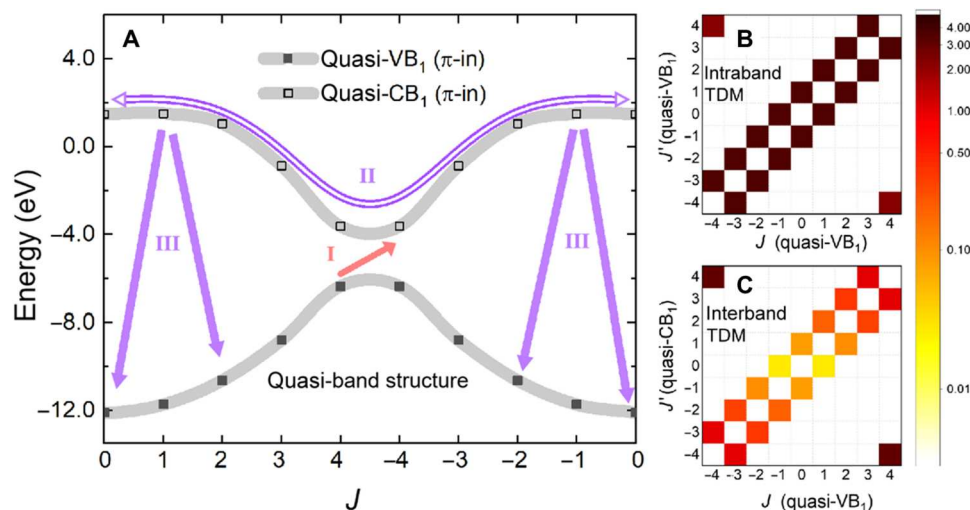


**Fig. 2. The quasienergy band structure and TDMs of polyynic cyclo[18]carbon in the framework of a generalized Bloch theorem with rotational invariance.** (A) The quasi-energy band structure with the interband transitions (I and III; solid arrows) and the intraband oscillations (II; hollow arrows) responsible for solid-like HHG. (B) The intraband and (C) interband TDM values. Here, the absolute values of (B) intraband TDMs for quasi-CB<sub>1</sub> (the values for quasi-VB<sub>1</sub> are almost the same as quasi-CB<sub>1</sub>) and (C) interband TDMs between quasi-VB<sub>1</sub> and quasi-CB<sub>1</sub> are shown. More data are available in the Supplementary Materials.

The cyclo[18]carbon is an all-carbon atomic ring composed of 18 carbon atoms. Since the earliest study in the 1960s by Hoffmann (15), its physical properties have been intensively explored including geometric structure (16) and electron correlations (17). Recently, a breakthrough in synthesis and characterization of cyclo[18]carbon has been achieved by Kaiser *et al.* (18, 19), which stimulated great interest because of the unique properties and potential applications of this cluster. Two kinds of geometric structures of cyclo[18]carbon have been taken into account in theoretical study: (i) A cumulenic structure with C—C bonds of equal length has a  $D_{18h}$  symmetry, and (ii) a polyynic structure with alternating triple and single bonds shows a  $D_{9h}$  symmetry. On the basis of the experimental findings (18, 19) and the theoretical corroboration of the higher stability of the polyynic structure (20, 21), we focused on the polyynic structure (i.e.,  $N = 9$ ), and the integer values of  $J$  are from  $-4$  to  $4$ .

## RESULTS

Because polyynic cyclo[18]carbon ( $D_{9h}$ ) is noncentrosymmetric, albeit spatial symmetry axis exists, a linearly polarized driving laser would lead to generation of both odd and even harmonics, which is dependent on the polarization direction of the incident light. In this work, we consider the lasers polarized linearly in the ring plane and use the following laser parameters: a wavelength of 1600 nm, a peak intensity of  $1.0 \times 10^{13}$  W/cm<sup>2</sup>, and a full width at half maximum of 45 fs. When the polarization of incident light is parallel to the symmetry axis of the target (Fig. 3A), the polarization directions of both odd and even harmonics are parallel to that of the incident laser. As shown in Fig. 3B, when the laser polarization is perpendicular to the symmetry axis, the polarization of the odd harmonics is parallel to that of the incident laser, while the polarization of the even ones is perpendicular to that of the driving laser. In contrast, cumulenic cyclo[18]carbon ( $D_{18h}$ ) is central inversion symmetric, and only odd-order harmonics with their polarization

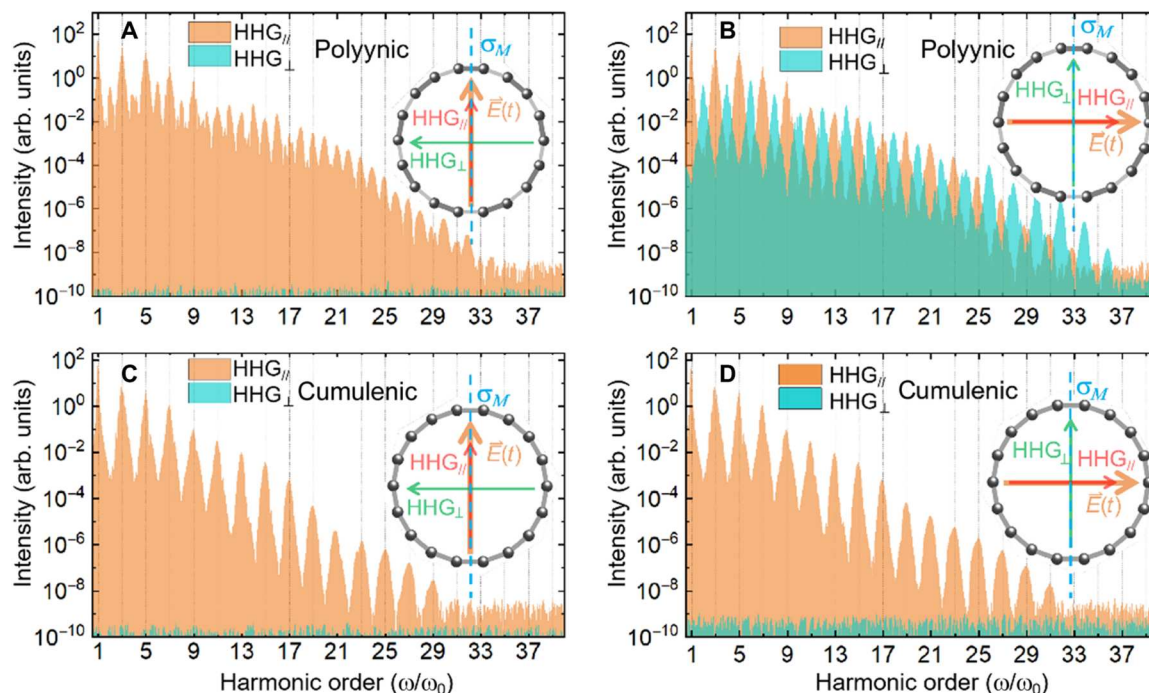


**Fig. 3. Simulated harmonic spectra of polyynic and cumulenic cyclo[18]carbon.** (A) For the electric field of driving laser parallel to the symmetry axis (shown as  $\sigma_M$ ). (B) For the electric field of driving laser perpendicular to the  $\sigma_M$  axis. (C) For the electric field of driving laser parallel to the  $\sigma_M$  axis. (D) For the electric field of driving laser perpendicular to the  $\sigma_M$  axis. In (A) to (D), the driving laser is linearly polarized, and the HHG parallel to the incident laser ( $\text{HHG}_{\parallel}$ ) and perpendicular to incident laser ( $\text{HHG}_{\perp}$ ) are depicted. The simulation is based on the quasi-band model including  $\pi$ -in and  $\pi$ -out bands. The laser wavelength of 1600 nm and the peak intensity of  $1.0 \times 10^{13}$  W/cm<sup>2</sup> are used.

parallel to the incident laser can be emitted, regardless whether the linearly polarized driving laser is parallel or perpendicular to the symmetry axis of cumulenic structure, as illustrated in Fig. 3 (C and D).

From Fig. 2 (B and C) and tables S1 to S6, electrons are excited via the transition from quasi-valence band (quasi-VB) maximum to quasi-conduction band (quasi-CB) minimum; subsequently, the main movement of the electrons under an external laser field should be the intraband oscillation because of the much larger intraband transition dipole moment (TDM) values, and the lower-order harmonics dominantly come from the intraband oscillation. When the electrons transit back to the quasi-VB following the selection rule, the interband emission may happen and generate a photon with higher energy. Although the interband TDMs nearby the diagonal squares are much smaller, the higher orders in the harmonic spectrum are mainly originated from the interband processes. To verify this, we perform additional calculations by removing such small interband TDMs nearby the diagonal squares in tables S5 and S6. The results shown in Fig. 4 (A to C) indicate that the harmonic intensity at high orders ( $>10$ ) are obviously reduced. Furthermore, we performed the time-frequency analysis of the HHG spectra. The results corresponding to the cases in Fig. 3 (A and C) are shown in fig. S5 (A and B, respectively). In fig. S5A, the low-order harmonics ( $\leq 7$ ) of polyynic cyclo[18]carbon are generated continuously in the time domain, which originate mainly from the intraband processes. By contrast, the higher-order harmonics of the polyynic structure are generated separately in each optical cycle, which are the clear characteristics of interband transitions. In fig.

S5B, the time-frequency analysis indicates that merely intraband harmonics can be generated for the cumulenic structure because of the special quasi-energy band (fig. S3).

To justify the validation of our quasi-band model, we performed extra calculations based on time-dependent density functional theory (TDDFT) (22). The harmonic spectra calculated by TDDFT calculations for polyynic and cumulenic structures are shown in Fig. 5. Because the TDDFT result relies on the chosen density functional and also presents fluorescent radiation that could be mixed with low-energy harmonic emission, here we focus on the high-order ( $\geq 13$ ) harmonics to unambiguously elucidate the essential odd-even features originated from the spatial symmetry of the cyclo[18]carbon molecule. In Fig. 5 (A to D) for both polyynic and cumulenic structures, TDDFT calculations well reproduce the main characteristics of odd- and even-order harmonics found by the quasi-band model, which are also consistent with that observed in other noncentrosymmetric systems of mirror axis such as the hydrogen-deuterium (HD) molecule (23), carbon monoxide (24), and monolayer MoS<sub>2</sub> (4, 25).

Moreover, the wavelength-dependent harmonic spectra calculated by the quasi-band model and the TDDFT method are shown in Fig. 6. Note that the fluorescent signals can also be seen in the TDDFT-simulated spectra. As the laser wavelength ( $\lambda$ ) increases, the cutoff value slightly decreases, which is different from the HHG in atoms ( $E_{\text{cutoff}} \propto \lambda^2$ ) but is closer to the characteristic of HHG in solids where the cutoff energy is independent on  $\lambda$ . Also, note that the quasi-energy bands are still discrete because of the limited number of atoms; thus, as the wavelength increases, the

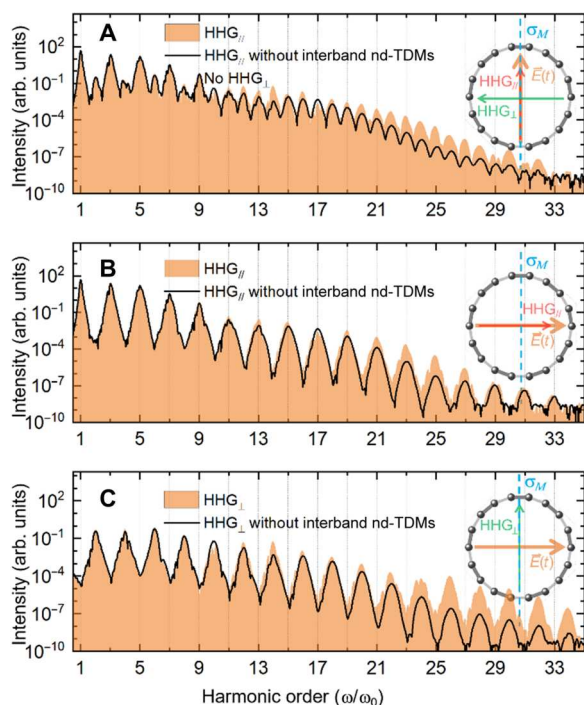


**Fig. 4.** HHG spectra of a polyynic structure calculated using the quasi-band model with and without the nearby diagonal TDMs (nd-TDM) of interband transitions. (A) For the laser polarization direction parallel to the symmetry axis. (B) The HHG parallel to the incident laser ( $\text{HHG}_{\parallel}$ ) with the laser polarization direction perpendicular to the symmetry axis. (C) The HHG perpendicular to incident laser ( $\text{HHG}_{\perp}$ ) with the laser polarization direction perpendicular to the symmetry axis. When the nd-TDMs (tables S5 and S6) are neglected, the intensities of the high-order ( $>18$ ) harmonics are decreased in (A) to (C). The laser wavelength of 1600 nm and the peak intensity of  $1.0 \times 10^{13} \text{ W/cm}^2$  are used.

electron along the quasi-energy band in discrete  $J$  space (Fig. 2A) becomes complex, which is different from the case of the crystal solids where electrons oscillate following the continuous band dispersion in  $k$  space. In Fig. 7, the simulated harmonic spectra dependent on the laser intensity ( $I$ ) by the quasi-band model and the TDDFT method are presented. As the laser intensity increases, the cutoff values satisfy the  $I^{1/2}$  relationship [as shown by the dashed lines in Fig. 7 (A and B)], which, once again, confirms the solid state-like HHG from the cyclo[18]carbon cluster.

## DISCUSSION

So far, for the gaseous atoms or molecules, HHG is usually analyzed based on the three-step ionization-acceleration-recollision process. The theory of solid-state HHG has made rapid progress; a similar “excitation–acceleration (Bloch oscillation)–recombination” process for solid HHG is based on the band theory. However, the theory of solid HHG has not yet been fully developed. For the material between solids and atoms, their HHG mechanism seems interesting. Here, we developed a theoretical model to study the interaction between the ultrafast strong laser and the cluster molecular systems satisfying rotational PBC. Because of the similarity with the HHG in the solid-state crystals governed by their band dispersions that can be theoretically simulated by solving

semiconductor Bloch equations, we denote it solid state-like HHG in the framework of a generalized Bloch theorem. Taking cyclo[18]carbon as an example, we confirm its interband and intraband mechanisms of HHG based on quasi-energy bands. Some pioneering studies (26, 27) have addressed the analogy between atomic HHG and solid-state HHG clearly. A recent atomic-like HHG study of two-dimensional materials (6) provides a more direct comparison with the atomic systems. The solid state-like HHG of ring-type clusters is from reverse thinking that has enriched the understanding of the HHG field. The theory and findings in this work are hopefully extended to other ring-type or ball-type molecules/clusters, nanotubes, or artificial metamaterials with rotational and translational PBCs that deserve much endeavor in the future.

## MATERIALS AND METHODS

Quantum chemistry calculations for electronic structures were carried out by the Gaussian 16 package (28), and the M06-2X functional with a basis set of 6-31G++(d,p) was used. The geometry of polyynic cyclo[18]carbon was optimized with the alternating bond lengths of 1.226 and 1.346 Å and all 18 C–C–C angles fixed at 160°, in good agreement with the reported values (20). The calculated gap between the highest occupied molecular orbital (MO) and the lowest unoccupied MO by a correction method (29) is 2.72 eV, implying that the polyynic cyclo[18]carbon is a semiconductor.

As is well understood, polyynic cyclo[18]carbon consists of two sets of 18-center delocalized  $\pi$  electrons (called  $\pi$ -in and  $\pi$ -out) with 18 occupied MOs and 18 unoccupied ones. To satisfy Eq. 1 perfectly, we perform a linear transformation for the energy-degenerated MOs as  $\psi_{\pm J} = \phi_j^a \pm i \phi_j^b$ , where  $\phi_j^a$  and  $\phi_j^b$  represent a couple of degenerated  $\pi$ -in (or  $\pi$ -out) MOs (see fig. S1). We divide 36  $\pi$ -in and  $\pi$ -out MOs into four bands according to their energies and corresponding  $J$  values. The quasi-energy band structures are presented in Fig. 2A and fig. S2. At the same  $J$  values, the occupied  $\pi$ -in and  $\pi$ -out bands are almost degenerated in energy while notable energy differences exist between the unoccupied ones. Here, we can regard the occupied band as the quasi-VB and the unoccupied one as the quasi-CB; thus, the four bands are named quasi-VB<sub>1</sub>, quasi-CB<sub>1</sub>, quasi-VB<sub>2</sub>, and quasi-CB<sub>2</sub>, in which the  $\pi$ -in bands have a subscript 1 and  $\pi$ -out bands have a subscript 2. Owing to the near equivalence between  $\pi$ -in and  $\pi$ -out VBs, in Fig. 2, we only present the properties of the  $\pi$ -in bands for clarity.

On the basis of Eq. 1, the TDM between the quasi-band pair for different  $J$  reads as

$$\vec{D}_{nn'}^{JJ'} = \langle \psi_{nj} | \vec{r} | \psi_{n'T'} \rangle \quad (2)$$

which satisfies the selection rule  $J - J' = \pm 1$  to ensure the conservation of angular momentum, and  $n/n'$  represents the band index. The calculated interband and intraband TDM values for  $\pi$ -in bands are shown in Fig. 2 (B and C, respectively). Note that the transitions between  $\pi$ -in and  $\pi$ -out bands are not allowed because of their different symmetry. The intraband TDM values nearby the diagonal squares in Fig. 2B are close to 3.5 atomic units (a.u.), corresponding to half of the radius of cyclo[18]carbon as  $\langle \psi_{nj} | x | \psi_{nj\pm 1} \rangle \approx \frac{1}{2\pi} \int_0^{2\pi} e^{-ij\theta} R_{c18} \cos\theta e^{i(j\pm 1)\theta} d\theta = \frac{R_{c18}}{2}$ , where  $R_{c18} \approx 7$  a.u. This property is also valid for larger rings such as cyclo[22]-carbon, cyclo[26]carbon, etc. In Fig. 2 (B and C), solid squares at the

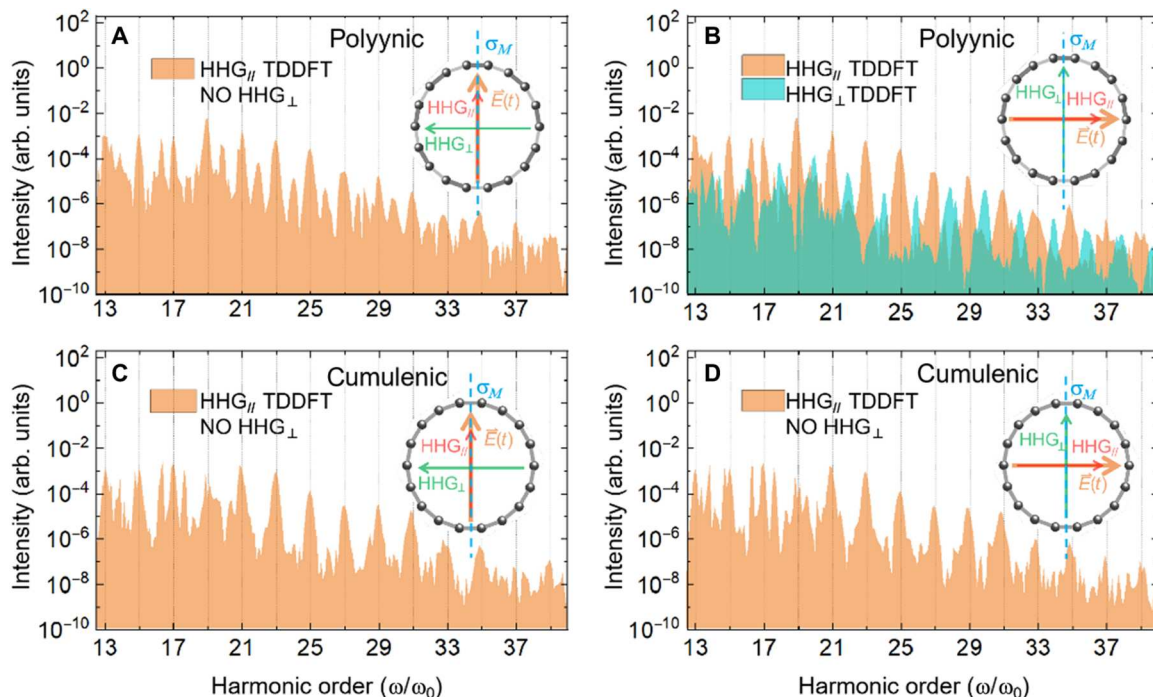


**Fig. 5. HHG spectra of polyynic and cumulenic structures calculated by the TDDFT method.** (A) For polyynic cyclo[18]carbon with the electric field of driving laser parallel to the symmetry axis crossing the center of two C—C bonds (shown as  $\sigma_M$ ). (B) For polyynic cyclo[18]carbon with the electric field of driving laser perpendicular to  $\sigma_M$ . (C) For cumulenic cyclo[18]carbon with the electric field of driving laser parallel to  $\sigma_M$ . (D) For cumulenic cyclo[18]carbon with the electric field of driving laser perpendicular to  $\sigma_M$ . The odd-even harmonic features corresponding to the incident polarizations are consistent with the results simulated by the quasi-band model. The laser wavelength of 1600 nm and the peak intensity of  $1.0 \times 10^{13}$  W/cm<sup>2</sup> are used.

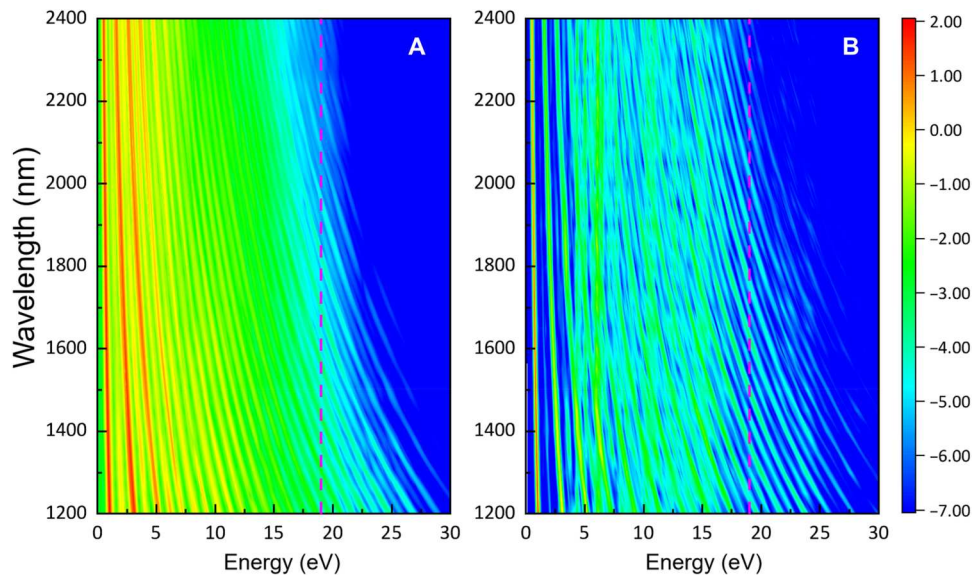


**Fig. 6. HHG spectra of a polyynic structure with different laser wavelengths.** The wavelength-dependent harmonic spectrum simulated by (A) the quasi-band model and (B) the TDDFT method. The peak intensity of the incident laser is fixed at  $1.0 \times 10^{13}$  W/cm<sup>2</sup>. The cutoff energy independent on laser wavelength in solid-state HHG is represented by the vertical dashed lines.

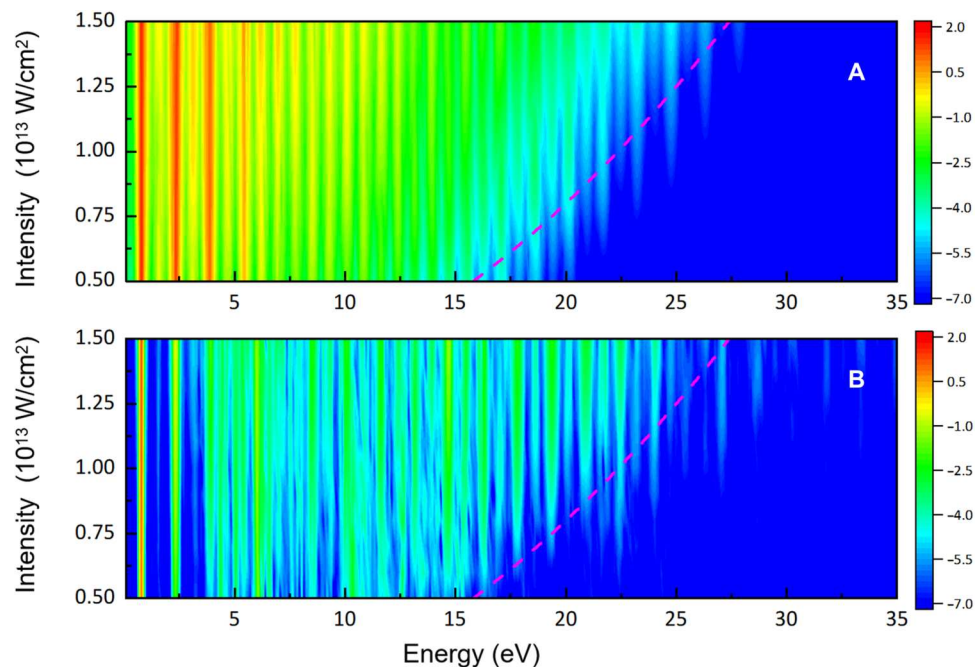


**Fig. 7. HHG spectra of a polyynic structure with different laser intensities.** The harmonic spectra simulated by (A) the quasi-band model and (B) the TDDFT method. The laser wavelength is fixed at 1600 nm. The cutoff energy follows the square root scaling law with respect to the laser intensity (dashed lines), which agrees with the intensity-dependent cutoff energy of solid-state HHG.

corners should be noticed, implying that the transition between  $J = -4$  and  $J = 4$  is allowed because of the rotationally periodic property.

To investigate the interaction between cyclo[18]carbon and the external laser field, we numerically solve the time-dependent Liouville–von Neumann equation

$$i\frac{\partial\rho}{\partial t} = [H, \rho] - \frac{\rho^d - \rho_0^d}{T_1} - \frac{\rho - \rho^d}{T_2} \quad (3)$$

where  $\rho$  represents the density matrix, and  $\rho^d$  and  $\rho_0^d$  are the diagonal term of  $\rho$  and the initial density matrix  $\rho_0$ , respectively.  $T_1$  is the relaxation time and  $T_2$  is the dephasing time. The Hamiltonian matrix is  $H = U_n^J + \vec{E}(t) \cdot \vec{D}_{nm}^J$ , where diagonal  $U_n^J$  is the quasi-energy band as shown in Fig. 2A and fig. S2,  $\vec{D}_{nm}^J$  is the abovementioned TDM, and  $\vec{E}(t)$  represents the time-dependent electric field of the driving laser. The time-dependent induced dipole  $\vec{P}(t) = \text{Tr}[\rho(t)\vec{D}]$  can be obtained through the density matrix, and then the HHG can be calculated from the Fourier transform of the dipole acceleration  $\vec{a}(t) = \ddot{\vec{P}}(t)$ . In principle, any system with rotational periodicity satisfying Eq. 1 (e.g., other ring-like clusters, supermolecules, nanotubes, or covalent organic frameworks) can form a quasi-energy band structure, and our model based on Eq. 3 is adaptable to simulate solid state-like HHG.

The TDDFT calculations were performed by the Octopus code (22) in which the time-dependent electronic current and the laser-induced electronic density were computed by propagating the Kohn-Sham equations in real space and real time in the adiabatic local density approximation (30). We used the fully relativistic Hartwigsen, Goedecker, and Hutter pseudo-potentials (31) and chose a

parallelepiped simulation box with the size of  $-(d/2 + 20) \text{ \AA} < x < d/2 + 20 \text{ \AA}$ ,  $-(d/2 + 20) \text{ \AA} < y < d/2 + 20 \text{ \AA}$  ( $d$  is the diameter of the cyclo[18]carbon), and  $-5 \text{ \AA} < z < 5 \text{ \AA}$ , including 15 \text{ \AA} of absorbing regions on each boundary of the  $x$  and  $y$  direction. The absorbing boundaries were treated using the complex absorbing potential (CAP) method, and the CAP height ( $\eta$ ) was taken as  $\eta = -0.2$  a.u. to avoid the reflection error in the spectral region of interest (32). The real-space cell was sampled with a grid spacing of 0.3 a.u. Moreover, the electronic density pulled away from the cyclo[18]carbon molecules was artificially absorbed by using a mask function for  $>5 \text{ \AA}$ ; i.e., the ionized electrons were excluded. Hence, the TDDFT calculations in the present work do not include the bound-continuum-bound transitions. For the moderate laser intensity ( $1.0 \times 10^{13} \text{ W/cm}^2$ ), the ionization probability is very low ( $<2 \times 10^{-5}$ ), which justifies the above approximation.

## Supplementary Materials

### This PDF file includes:

Figs. S1 to S6  
Tables S1 to S6  
References

## REFERENCES AND NOTES

1. P. M. Paul, E. S. Toma, P. Breger, G. Mullot, F. Augé, P. Balcou, H. G. Muller, P. Agostini, Observation of a train of attosecond pulses from high harmonic generation. *Science* **292**, 1689–1692 (2001).
2. P. B. Corkum, Plasma perspective on strong field multiphoton ionization. *Phys. Rev. Lett.* **71**, 1994–1997 (1993).
3. T. T. Luu, M. Garg, S. Y. Kruchinin, A. Moulet, M. T. Hassan, E. Goulielmakis, Extreme ultraviolet high-harmonic spectroscopy of solids. *Nature* **521**, 498–502 (2015).

4. H. Liu, Y. Li, Y. S. You, S. Ghimire, T. F. Heinz, D. A. Reis, High-harmonic generation from an atomically thin semiconductor. *Nat. Phys.* **13**, 262–265 (2017).
5. M. Garg, M. Zhan, T. T. Luu, H. Lakhota, T. Klostermann, A. Guggenmos, E. Goulielmakis, Multi-petahertz electronic metrology. *Nature* **538**, 359–363 (2016).
6. N. Tancogne-Dejean, A. Rubio, Atomic-like high-harmonic generation from two-dimensional materials. *Sci. Adv.* **4**, eaao520 (2018).
7. C. Yu, S. Jiang, T. Wu, G. Yuan, Y. Peng, C. Jin, R. Lu, Higher harmonic generation from bilayer nanostructures assisted by electron backscattering. *Phys. Rev. B* **102**, 241407 (2020).
8. S. Jiang, J. Chen, H. Wei, C. Yu, R. Lu, C. D. Lin, Role of the transition dipole amplitude and phase on the generation of odd and even high-order harmonics in crystals. *Phys. Rev. Lett.* **120**, 253201 (2018).
9. S. Jiang, S. Gholam-Mirzaei, E. Crites, J. E. Beetar, M. Singh, R. Lu, M. Chini, C. D. Lin, Crystal symmetry and polarization of high-order harmonics in ZnO. *J. Phys. B At. Mol. Opt. Phys.* **52**, 225601 (2019).
10. H. Ruf, C. Handschin, R. Cireasa, N. Thiré, A. Ferré, S. Petit, D. Descamps, E. Mével, E. Constant, V. Blanchet, B. Fabre, Y. Mairesse, Inhomogeneous high harmonic generation in krypton clusters. *Phys. Rev. Lett.* **110**, 083902 (2013).
11. H. Park, Z. Wang, H. Xiong, S. B. Schoun, J. Xu, P. Agostini, L. F. DiMauro, Size-dependent high-order harmonic generation in rare-gas clusters. *Phys. Rev. Lett.* **113**, 263401 (2014).
12. Y. C. Lee, W. Z. Lee, Rotational states of a benzenelike ring and Bloch's theorem. *Am. J. Phys.* **77**, 1144–1146 (2009).
13. O. O. Kit, L. Pastewka, P. Koskinen, Revised periodic boundary conditions: Fundamentals, electrostatics, and the tight-binding approximation. *Phys. Rev. B* **84**, 155431 (2011).
14. E. Dobardžić, M. Dimitrijević, M. V. Milovanović, Generalized Bloch theorem and topological characterization. *Phys. Rev. B* **91**, 125424 (2015).
15. R. Hoffmann, Extended hückel theory—V. *Tetrahedron* **22**, 521–538 (1966).
16. V. Parasuk, J. Almlöf, M. W. Feyereisen, The [18] all-carbon molecule: Cumulene or polycetylene? *J. Am. Chem. Soc.* **113**, 1049–1050 (1991).
17. T. Torelli, L. Mitás, Electron correlation in  $C_{4N+2}$  carbon rings: Aromatic versus dimerized structures. *Phys. Rev. Lett.* **85**, 1702–1705 (2000).
18. K. Kaiser, L. M. Scriven, F. Schulz, P. Gawel, L. Gross, H. L. Anderson, An sp-hybridized molecular carbon allotrope, cyclo[18]carbon. *Science* **365**, 1299–1301 (2019).
19. L. M. Scriven, K. Kaiser, F. Schulz, A. J. Sterling, S. L. Woltering, P. Gawel, K. E. Christensen, H. L. Anderson, L. Gross, Synthesis of cyclo[18]carbon via debromination of  $C_{18}Br_6$ . *J. Am. Chem. Soc.* **142**, 12921–12924 (2020).
20. G. V. Baryshnikov, R. R. Valiev, A. V. Kuklin, D. Sundholm, H. Ågren, Cyclo[18]carbon: Insight into electronic structure, aromaticity, and surface coupling. *J. Phys. Chem. Lett.* **10**, 6701–6705 (2019).
21. Z. S. Pereira, E. Z. da Silva, Spontaneous symmetry breaking in cyclo[18]carbon. *J. Phys. Chem. A* **124**, 1152–1157 (2020).
22. X. Andrade, D. Strubbe, U. De Giovannini, A. H. Larsen, M. J. T. Oliveira, J. Alberdi-Rodríguez, A. Varas, I. Theophilou, N. Helbig, M. J. Verstraete, L. Stella, F. Nogueira, A. Aspuru-Guzik, A. Castro, M. A. L. Marques, A. Rubio, Real-space grids and the Octopus code as tools for the development of new simulation approaches for electronic systems. *Phys. Chem. Chem. Phys.* **17**, 31371–31396 (2015).
23. T. Kreibich, M. Lein, V. Engel, E. K. U. Gross, Even-harmonic generation due to beyond-Born-Oppenheimer dynamics. *Phys. Rev. Lett.* **87**, 103901 (2001).
24. H. Hu, N. Li, P. Liu, R. Li, Z. Xu, Pure even harmonic generation from oriented CO in linearly polarized laser fields. *Phys. Rev. Lett.* **119**, 173201 (2017).
25. C. Liu, Y. Zheng, Z. Zeng, R. Li, Polarization-resolved analysis of high-order harmonic generation in monolayer  $MoS_2$ . *New J. Phys.* **22**, 073046 (2020).
26. G. Vampa, T. J. Hammond, N. Thiré, B. E. Schmidt, F. Légaré, C. R. McDonald, T. Brabec, D. D. Klug, P. B. Corkum, All-optical reconstruction of crystal band structure. *Phys. Rev. Lett.* **115**, 193603 (2015).
27. G. Vampa, T. J. Hammond, N. Thiré, B. E. Schmidt, F. Légaré, C. R. McDonald, T. Brabec, P. B. Corkum, Linking high harmonics from gases and solids. *Nature* **522**, 462–464 (2015).
28. M. J. Frisch, G. W. Trucks, H. B. Schlegel, G. E. Scuseria, M. A. Robb, J. R. Cheeseman, G. Scalmani, V. Barone, G. A. Petersson, H. Nakatsuji, X. Li, M. Caricato, A. V. Marenich, J. Bloino, B. G. Janesko, R. Gomperts, B. Mennucci, H. P. Hratchian, J. V. Ortiz, A. F. Izmaylov, J. L. Sonnenberg, D. Williams-Young, F. Ding, F. Lipparini, F. Egidi, J. Goings, B. Peng, A. Petrone, T. Henderson, D. Ranasinghe, V. G. Zakrzewski, J. Gao, N. Rega, G. Zheng, W. Liang, M. Hada, M. Ehara, K. Toyota, R. Fukuda, J. Hasegawa, M. Ishida, T. Nakajima, Y. Honda, O. Kitao, H. Nakai, T. Vreven, K. Throssell, J. A. Montgomery, Jr., J. E. Peralta, R. Ogliaro, M. J. Bearpark, J. J. Heyd, E. N. Brothers, K. N. Kudin, V. N. Staroverov, T. A. Keith, F. Kobayashi, J. Normand, K. Raghavachari, A. P. Rendell, J. C. Burant, S. S. Iyengar, J. Tomasi, M. Cossi, J. M. Millam, M. Klene, C. Adamo, R. Cammi, J. W. Ochterski, R. L. Martin, K. Morokuma, O. Farkas, J. B. Foresman, D. J. Fox, Gaussian 16 Revision C.01 (Gaussian, Inc., 2016).
29. M. Li, Z. Gao, Y. Han, Y. Zhao, K. Yuan, S. Nagase, M. Ehara, X. Zhao, Potential molecular semiconductor devices: Cyclo-C: n ( $n = 10$  and  $14$ ) with higher stabilities and aromaticities than acknowledged cyclo-C18. *Phys. Chem. Chem. Phys.* **22**, 4823–4831 (2020).
30. G. Onida, L. Reining, A. Rubio, Electronic excitations: Density-functional versus many-body Green's-function approaches. *Rev. Mod. Phys.* **74**, 601–659 (2002).
31. C. Hartwigsen, S. Goedecker, J. Hutter, Relativistic separable dual-space Gaussian pseudopotentials from H to Rn. *Phys. Rev. B* **58**, 3641–3662 (1998).
32. U. De Giovannini, A. H. Larsen, A. Rubio, Modeling electron dynamics coupled to continuum states in finite volumes with absorbing boundaries. *Eur. Phys. J. B* **88**, 56 (2015).
33. O. E. Alon, V. Averbukh, N. Moiseyev, Selection rules for the high harmonic generation spectra. *Phys. Rev. Lett.* **80**, 3743–3746 (1998).
34. A. Fleischer, O. Kfir, T. Diskin, P. Sidorenko, O. Cohen, Spin angular momentum and tunable polarization in high-harmonic generation. *Nat. Photonics* **8**, 543–549 (2014).
35. F. Ceccherini, D. Bauer, F. Cornolti, Dynamical symmetries and harmonic generation. *J. Phys. B At. Mol. Opt. Phys.* **34**, 5017–5029 (2001).

**Acknowledgments:** We thank P. Liu, S. Wu, and F. Song for helpful discussions. **Funding:** This work was supported by the NSF of China (grant nos. 12174195, 12074124, 11974185, 11904028, and 11834004), National Institutes of Health grant R01AB123456 (PV, GS), the Natural Science Foundation of Jiangsu Province (grant no. BK20170032), and the National Key Research and Development Program of China (no. 2022YFA1604301). **Author contributions:** Conceptualization: C.Y., R.L., and K.D. Methodology: Y.P., C.Y., T.W., and G.Y. Investigation: Y.P., C.Y., S.J., and G.Y. Visualization: Y.P., L.C., and T.W. Supervision: R.L. and K.D. Writing—original draft: Y.P., R.L., and C.Y. Writing—review and editing: R.L. and K.D. **Competing interests:** The authors declare that they have no competing interests. **Data and materials availability:** All data needed to evaluate the conclusions in the paper are present in the paper and/or the Supplementary Materials. Codes and scripts sufficient to further verify this paper's results are deposited at <https://dx.doi.org/10.5061/dryad.3j9kd51np>. See the Supplementary Materials for details.

Submitted 27 June 2022

Accepted 19 January 2023

Published 17 February 2023

10.1126/sciadv.add6810